

Article

Understanding High-Energy (UV and X-ray) Emission from AGB Stars—Episodic Accretion in Binary Systems

Raghvendra Sahai ^{1,*}, Jorge Sanz-Forcada ², Martin Guerrero ³, Roberto Ortiz ⁴
and Carmen Sanchez Contreras ²

¹ Jet Propulsion Laboratory, California Institute of Technology, Pasadena, CA 91109, USA

² Centro de Astrobiología (CSIC-INTA), ESAC Campus, 28691 Villanueva de la Cañada, Spain; jsanz@cab.inta-csic.es (J.S.-F.); csanchez@cab.inta-csic.es (C.S.C.)

³ Instituto de Astrofísica de Andalucía, 18008 Granada, Spain; mar@iaa.es

⁴ Escola de Artes, Ciências e Humanidades, USP, Sao Paulo 03828-000, Brazil; rortiz@usp.br

* Correspondence: sahai@jpl.nasa.gov; Tel.: +1-818-354-0452

Abstract: X-ray surveys of UV-emitting AGB stars show that $\sim 40\%$ of objects with FUV emission and GALEX FUV/NUV flux ratio $R_{fuv/nuv} \gtrsim 0.2$ (fuvAGB stars) have variable X-ray emission characterized by very high temperatures ($T_x \sim 35\text{--}160$ MK) and luminosities ($L_x \sim 0.002\text{--}0.2 L_\odot$), indicating the presence of accretion associated with a close binary companion. However, the UV-emitting AGB star population is dominated by objects with $R_{fuv/nuv} \lesssim 0.06$ (nuvAGB stars), and we do not know whether the UV emission from these is intrinsic to the AGB star or extrinsic (i.e., due to binarity). In order to help distinguish between intrinsic and extrinsic models of the puzzling high-energy emission of cool AGB stars, we report results from two studies—(i) XMM-Newton X-observations of two nuvAGB stars, and (ii) simple chromosphere modeling. In study (i), we detect the one which has the lower FUV/NUV ratio, with a total $L_x = 0.00027 L_\odot$, and a spectrum best fitted with a dominant component at $T_x \sim 10$ MK, most likely coronal emission from a main-sequence companion. Therefore, a significant fraction of nuvAGB stars may also be binaries with active, but weak accretion. Study (ii) shows that chromospheres with temperatures of $\sim 10,000$ K can produce $R_{fuv/nuv} \lesssim 0.06$; higher ratios require hotter gas, implying active accretion.

Keywords: circumstellar matter; binaries (including multiple); close; stars: evolution; stars: AGB and post-AGB; stars: mass loss; wavelengths: UV; X-ray



Citation: Sahai, R.; Sanz-Forcada, J.; Guerrero, M.; Ortiz, R.; Contreras, C.S. Understanding High-Energy (UV and X-ray) Emission from AGB Stars—Episodic Accretion in Binary Systems. *Galaxies* **2022**, *10*, 62. <https://doi.org/10.3390/galaxies10030062>

Academic Editor: Artemio Herrero

Received: 7 February 2022

Accepted: 5 April 2022

Published: 25 April 2022

Publisher's Note: MDPI stays neutral with regard to jurisdictional claims in published maps and institutional affiliations.



Copyright: © 2022 by the authors. Licensee MDPI, Basel, Switzerland. This article is an open access article distributed under the terms and conditions of the Creative Commons Attribution (CC BY) license (<https://creativecommons.org/licenses/by/4.0/>).

1. Introduction

Stars in the $1\text{--}8 M_\odot$ range expel half or more of their masses at rates up to $\sim 10^{-4} M_\odot \text{ yr}^{-1}$ (e.g., Decin 2021 [1], Olofsson 2008 [2]), as they evolve from the asymptotic giant branch (AGB) to the preplanetary nebula (PPN) and planetary nebula (PN) evolutionary phases. This mass loss dramatically alters the course of stellar evolution, enriches the interstellar medium (ISM) with nucleosynthetically enriched material and thus plays a key role in the chemical evolution of galaxies. AGB stars also eject copious quantities of dust grains into the ISM, which are crucial ingredients for the birth of new Sun-like stars and solar systems. Young PNe (YPNe) represent the bright end-stages of these stars and provide valuable diagnostics on their demise. However, YPNe formation and the phase of extreme mass loss at the end of the AGB phase is very poorly understood—although the mass ejection in the latter is generally spherical, producing extended circumstellar envelopes (CSEs) expanding at speeds of $10\text{--}20 \text{ km s}^{-1}$, all observed PPNe and most YPNe are observed to have bipolar, multipolar or elliptical shapes (e.g., Sahai and Trauger 1998 [3] [ST98], Sahai et al. 2007 [4], Sahai et al. 2011 [5] [SMV11]). Collimated high-speed outflows ($\gtrsim 50\text{--}100 \text{ km s}^{-1}$) are ubiquitous during the PPN phase (Bujarrabal et al. 2001 [6]).

Morphologically unbiased HST imaging surveys have observationally bracketed the evolutionary phases that cover the transition from the spherical to aspherical morphology.

These surveys imaged (1) nascent PPNe (IRAS 25–12 μm flux ratio $1 < F_{25}/F_{12} < 1.4$, to select for objects lacking hot dust, as an indicator that dense AGB mass loss is decreasing) (Sahai et al. 2006 [7]), (2) PPNe ($F_{25}/F_{12} > 1.4$, to select for objects lacking warm dust, as an indicator that dense AGB mass loss has stopped recently) (Sahai et al. 2007 [4]), and (3) YPNe (i.e., compact, with size $\lesssim 10''$, and the flux ratio $[\text{OIII}]/\text{H}\alpha \lesssim 1$) (ST98, SMV11). The PPN and YPN surveys led to a systematic characterization scheme for the observed morphologies with four primary classes (B: bipolar, M: multipolar, E: elongated, and I: irregular) (e.g., Figure 1a–h). No round PPN was found. Nascent PPNe look morphologically different from PPNe and YPNe, typically showing asymmetric elongated structures (Figure 1j,k). Such structures could result from either (a) an aspherical density distribution, and/or (b) aspherical illumination. Case (b) would require the presence of relatively low-density channels close to the central star, which allow the starlight to escape preferentially along specific directions, and illuminate more distant regions of the circumstellar medium in an aspherical manner. In either case, the mechanism for creating the large-scale density inhomogeneities is likely to be a high-velocity outflow that has just begun to sculpt the innermost regions of the AGB mass-loss envelope.

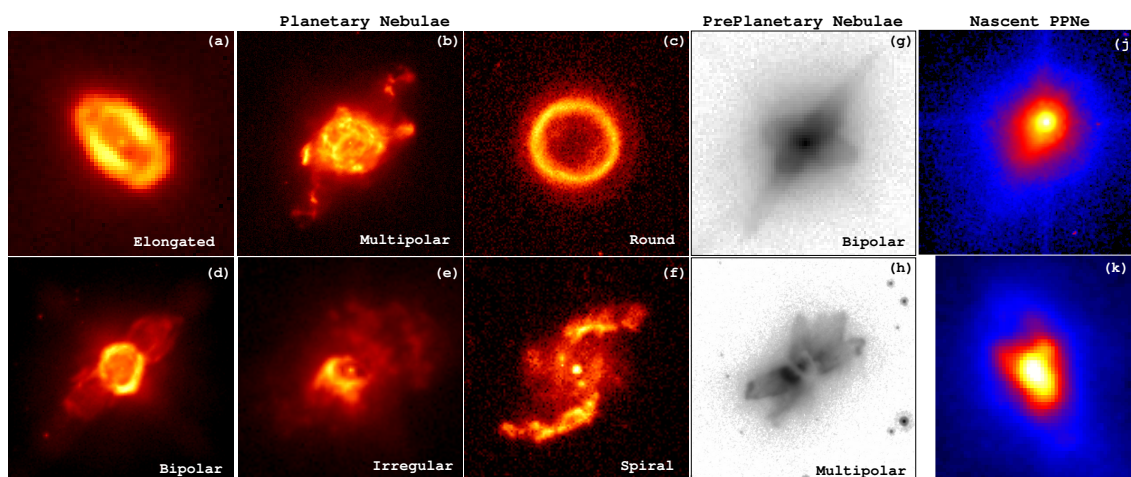


Figure 1. YPNe, PPNe, and nascent PPNe images from HST—(a–f) $\text{H}\alpha$ (or $[\text{NII}]$) images of PNe belonging to 6 primary classes in the Sahai, Morris, and Villar (2011) [5] classification system, which consists of 7 primary classes based on the overall nebular shape, and several categories of secondary characteristics related to specific properties of the lobes, waist, and haloes, and the presence of point-symmetry; (g,h) $0.6 \mu\text{m}$ images of PPNe belonging to 2 primary classes; and (j,k) $0.6 \mu\text{m}$ images of nascent PPNe. (a) PNG 014.3 – 05.5 ($4''.0 \times 4''.0$), (b) PNG 027.6 – 09.6 ($11''.4 \times 11''.4$), (c) PNG 357.2 + 02.0 ($2''.67 \times 2''.67$), (d) PNG 356.5 – 03.9 ($6''.84 \times 6''.84$), (e) PNG 068.3 – 02.7 ($3''.8 \times 3''.8$), (f) PNG 032.1 + 07.0 ($4''.67 \times 4''.67$), (g) IRAS 04296 + 3429 ($3''.7 \times 3''.7$), (h) IRAS 19024 + 0044 ($6''.3 \times 6''.3$), (j) IRAS 23320 + 4316 ($0''.48 \times 0''.48$), and (k) IRAS 15082-4808 ($0''.69 \times 0''.8$).

So what is the underlying cause (or causes) of this dramatic AGB-to-PN transition? Binary interactions, directly or indirectly, are now widely believed to be the culprit. These include common-envelope ejection (Ivanova et al. 2013 [8]) or grazing envelope evolution (Soker 2015 [9]) and/or accretion disk and torus formation, or indirectly via increased rotation and the generation of strong magnetic fields (e.g., Blackman et al. 2001 [10]). Binaries provide a source of angular momentum and free energy to form accretion disks and such disks can in turn amplify magnetic fields that can transport angular momentum on large scales (Blackman and Lucchini 2014 [11]). The latter process can result in high-speed, collimated jet-like outflows that sculpt the surrounding spherical circumstellar envelopes from the inside out during the late AGB or early PPN phase, producing bipolar and multipolar shapes (ST98). Yet most of our current understanding of this late evolutionary stage is based on single-star models! One reason for this is the lack of observational evidence for close binary companions in AGB stars. AGB stars are very luminous and

variable, invalidating standard techniques for binary detection (e.g., radial-velocity and photometric variations due to a companion star and direct imaging.) Interestingly, the long secondary periods found for many RGB and AGB stars provides possible new evidence for the presence of close companions (Wood et al. 1999 [12], Soszyński et al. 2021 [13]).

2. UV and X-ray Emission as a Probe of Binarity

2.1. UV Emission

Sahai et al. (2008) [14] were the first to show that UV observations can be used to search for binarity and associated accretion activity in AGB stars because most of these are relatively cool ($T_{eff} \lesssim 3000$ K) objects (spectral types $\sim M6$ or later), whereas any stellar companions and/or accretion disks around them are likely significantly hotter ($T_{eff} \gtrsim 6000$ K), so that favorable secondary-to-primary flux contrast ratios ($\gtrsim 10$) are reached in the GALEX FUV (1344–1786 Å) and NUV (1771–2831 Å) bands for a source (companion or disk) with $T_{eff} \gtrsim 6000$ K and luminosity $L \gtrsim 1 L_{\odot}$. From an application of this technique to a volume-limited sample (< 0.5 kpc) of 58 AGB stars, Ortiz, and Guerrero (2016) [15] conclude that the detection of FUV emission or an observed-to-predicted ratio for NUV emission of $Q_{NUV} > 20$ are criteria for binarity.

UV spectroscopy can provide an unambiguous probe of accretion-related activity because the latter is expected to produce UV lines with large widths and large Doppler shifts. An HST/STIS spectroscopic study of the prototype fuvAGB star, Y Gem, shows the presence of high-velocity infalling and outflowing material as well as flickering, and thus directly supports the binary/accretion hypothesis (see Figure 2 and Sahai et al. 2018 [16]). The UV spectrum of Y Gem shows lines from species such as Si IV and C IV (Figure 2a), with broad emission and absorption features (FWHM ~ 300 – 700 km s $^{-1}$) that are, respectively, red- and blue-shifted by velocities of ~ 500 km s $^{-1}$ from the systemic velocity. The UV continuum reveals strong flickering on time scales of $\lesssim 20$ s (Figure 2c), characteristic of an active accretion disk with an accretion hot spot of size $\lesssim 0.1$ au. A two-blackbody model that fits the G140L and G230L spectra shows significant variations in the luminosity (Figure 2d), but not in the temperature. Since neither of these two blackbodies fit the properties of a viable stellar companion (WD or MS) to the primary, it is likely that both the hot and cool UV components arise in a hot accretion disk, which results from the gravitational capture of material from the primary star by a low-mass main-sequence companion. A simple geometric model can then qualitatively explain the Doppler shifts of the absorption and emission features observed in the UV spectra: the accretion disk captures part of the material in an outflow or Roche-lobe overflow from the primary AGB star, via two possible infall streams—these produce red-shifted emission features. Assuming that the total luminosity of the blackbody components, $L_{acc} = 13 L_{\odot}$, results from accretion, the mass accretion rate resulting from the infall is $L_{acc} R_c / G M_c \gtrsim 5 \times 10^{-7} M_{\odot} \text{ yr}^{-1}$, where $R_c = 0.44 R_{\odot}$ and $M_c = 0.35 M_{\odot}$ are the radius and mass of the companion (Sahai et al. 2015 [17]), and G is the gravitational constant. The accretion disk powers a fast outflow that absorbs UV photons from the disk, producing blue-shifted absorption features.

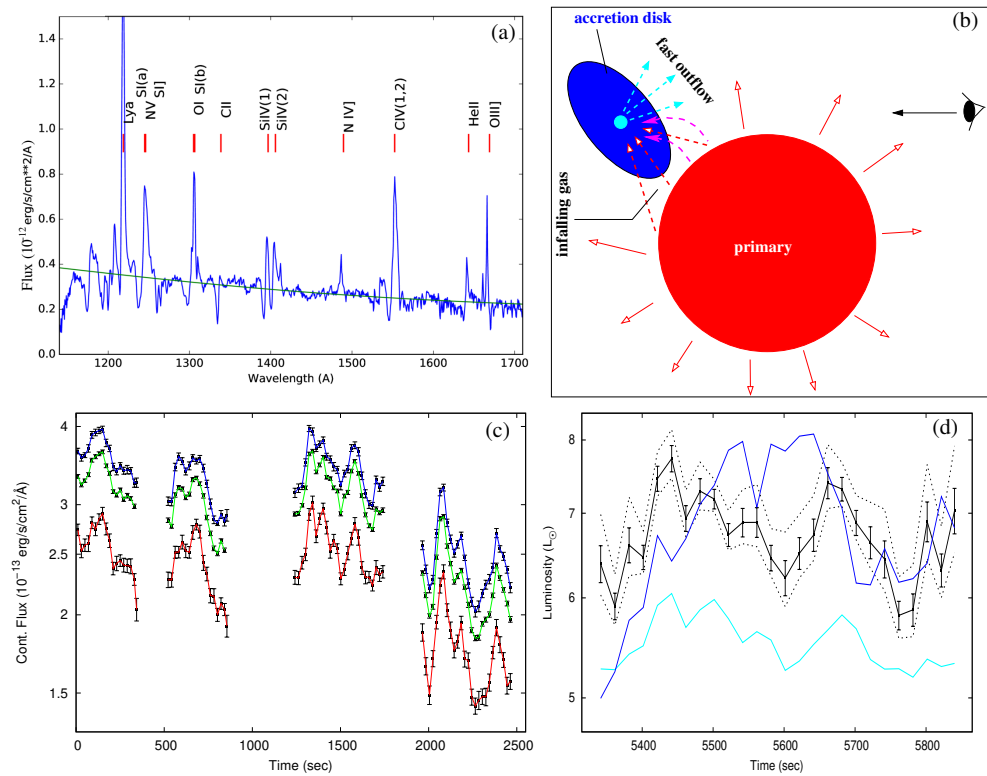


Figure 2. (a) STIS/UV spectrum of Y Gem and model fit (green curve) consisting of two blackbody components— $T_{\text{eff}} = 35,500$ K, $L = 6.3 L_{\odot}$ and $T_{\text{eff}} = 9400$ K, $L = 6.7 L_{\odot}$. (b) Schematic model geometry (not to scale) to explain the Doppler shifts of the absorption and emission features observed in the UV spectra: the blue ellipse shows an accretion disk around a compact companion; dashed red/pink arrows show two possible infall streams resulting from material in an outflow or Roche-lobe overflow (red arrows) from the primary AGB star (red circle); (c) short-term time variations in the (c) FUV continuum: line-free continuum in the bands 1346–1367 Å (blue) and 1571–1600 Å (red), continuum underlying the Si IV(1) line (green), and (d) short-term time variations in the luminosity (black) of the high-temperature accretion component: the dashed curves show bounds on the luminosity due to the estimated uncertainties in the cooler blackbody's luminosity and temperature. The 1571–1600 Å continuum, scaled up by a factor 1.1×10^7 (cyan), and the square-root of the Si IV(1) absorption line equivalent width, scaled up by a factor 5.2 (blue), are shown for comparison (*adapted from Sahai et al. (2018) [16]*).

2.2. X-ray Emission

The detection of X-rays towards AGB stars provides strong supporting evidence for accretion activity. An AGB star is unlikely to be a source of X-ray emission, since it would require rather strong magnetic fields to confine the hot plasma, and sensitive searches for X-rays in two AGB stars with strong magnetic fields have been unsuccessful (Kastner and Soker 2004 [18]), but it cannot be ruled out. Alternatively, a secondary component would provide the X-ray flux from AGB stars, either originating in an accretion disk around the secondary, or in the corona of an MS companion.

X-ray-emitting AGB stars have been found both in targeted X-ray searches in selected samples of AGB stars with high values (>0.17) of $R_{fuv/nuv}$ (Sahai et al. 2015 [9]) as well as serendipitous detections in an archival survey (Ortiz and Guerrero 2021 [19]). The X-ray emission is variable, both on long (Figure 3) and short (Figure 4) time scales and may be related to variations in the accretion-flow and/or the circumstellar absorbing column. The short-term variability is similar to the flickering observed in the STIS study of Y Gem (see above). The Astrophysica Plasma Emission Code (APEC; Smith et al. 2001 [20]) was used to fit the X-ray spectra of five sources with the highest S/N X-ray spectra (two of these are shown in Figure 3). We find that the observed X-ray luminosity (L_x) and

temperature (T_x) lie in the range $L_x \sim (0.002\text{--}0.2) L_\odot$ and $T_x \sim (3.5\text{--}16) \times 10^7$ K. The high X-ray temperatures argue against the emission arising in stellar coronae, and the high X-ray luminosities specifically argue against emission originating in the coronae of main-sequence companions for the high $R_{fuv/nuv}$ AGB stars observed by Sahai et al. (2015) [17].

There is strong evidence that the X-ray emission is associated with the far-UV flux, and both result from accretion activity. We find that $R_{fuv/nuv}$ is a better indicator of X-ray emission than the FUV (or NUV) flux alone. For example, when AGB stars are classified into fuvAGB (i.e., those with the GALEX FUV/NUV ratio $R_{fuv/nuv} > 0.15$) and nuvAGB ($R_{fuv/nuv} < 0.06$), we observe that X-ray emission has been detected only in fuvAGB stars with $R_{fuv/nuv} > 0.17$ (including two ROSAT detections reported by Ramstedt et al. 2012 [21]) (see Figure 4b in Sahai et al. 2015 [17]).

The far-UV and near-UV emission might have different origins. For instance, Montez et al. (2017) [22] found that the GALEX near-UV magnitude follows the stellar pulsation (i.e., it is intrinsic, likely dominated by chromospheric emission from the AGB star), whereas the far-UV does not show this correlation, and its more likely to be extrinsic, likely dominated by emission from an accretion disk.

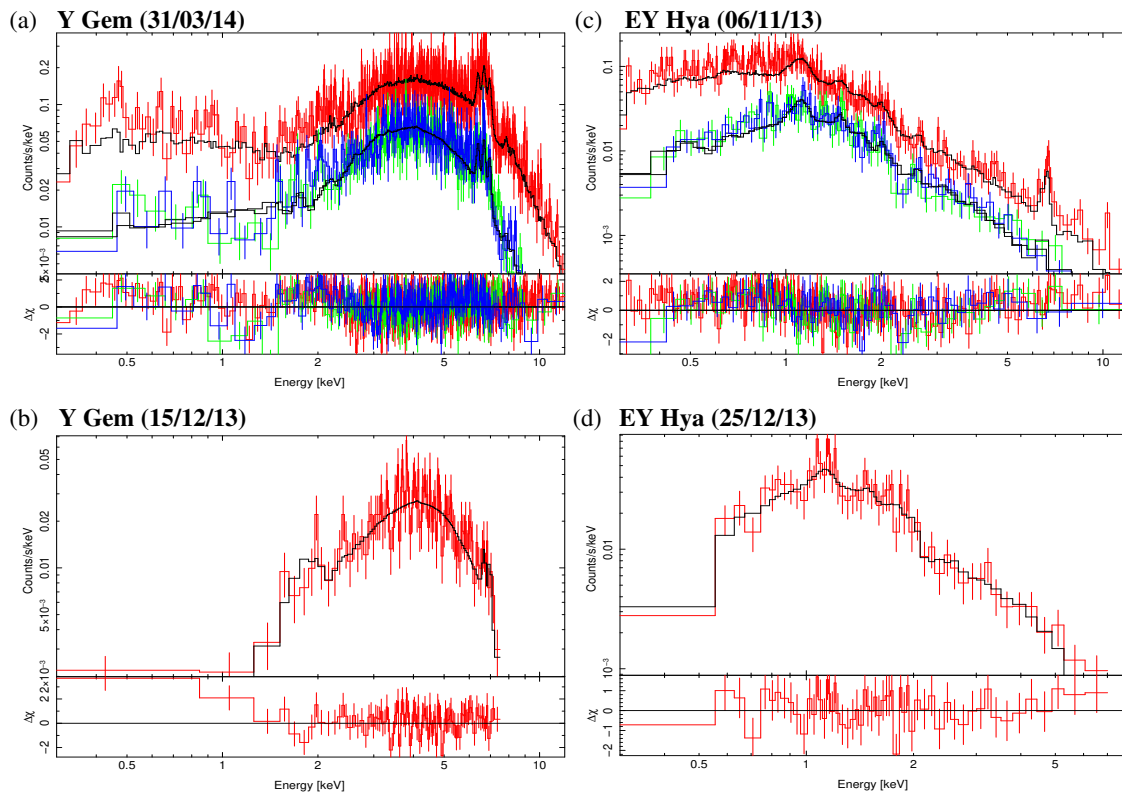


Figure 3. X-ray spectra (colored curves) for the fuvAGB stars Y Gem and EY Hya, taken at/different epochs/observatories+instruments, together with APEC model fits (black curves): (a) Y Gem (31/03/14: XMM-Newton), (b) Y Gem (15/12/13: CXO), (c) EY Hya (06/11/13: XMM-Newton), and (d) EY Hya (25/12/13: CXO). XMM (EPIC = pn + MOS1 + MOS2) data are shown as follows – pn: red, MOS1: green, MOS2: blue. CXO (ACIS-S) data are shown as red curves. The model X-ray luminosity (L_x), temperature (T_x), and absorbing column density (N_H) are, (i) for Y Gem: $L_x = 0.226$ (0.115) L_\odot , $T_x = 10^{8.1}$ ($10^{8.2}$) K, and $N_H = 8.13$ (15.6) $\times 10^{22}$ cm^{-2} for epoch 31/03/14 (15/12/13), and (i) for EY Hya: $L_x = 0.0024$ (0.002) L_\odot , $T_x = 10^{7.74}$ ($10^{7.57}$) K, and $N_H = 0.05$ (0.095) $\times 10^{22}$ cm^{-2} for epoch 25/12/13 (06/11/13) (adapted from Sahai et al. (2015) [17]).

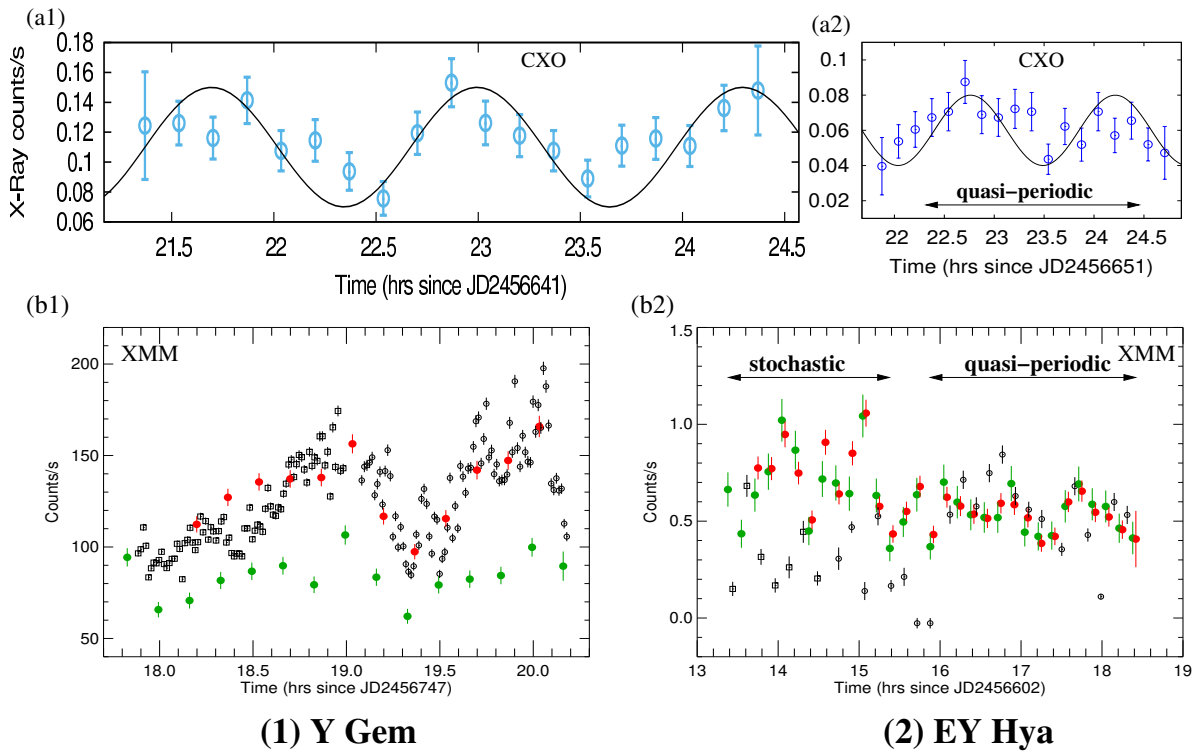


Figure 4. Short-term X-ray and UV variability in the fuvAGB stars Y Gem and EY Hya. Panels (a1,a2) show the X-ray light curves for Y Gem and EY Hya obtained with CXO (ACIS-S), respectively. Panels (b1,b2) show the X-ray and UV light curves for Y Gem and EY Hya obtained with XMM (EPIC = pn + MOS1 + MOS2: red, MOS = MOS1 + MOS2: green, UVM2: black squares, UVW2: black circles), respectively. The EPIC, MOS and UVW2 data have been rescaled. Nonlinear least-squares sinusoidal fits with periods, $p = 1.35$ h and 1.45 h are shown for the X-ray light curves of Y Gem and EY Hya in panels (b1,b2); the respective uncertainties in the periods are ± 0.026 h and ± 0.055 h (adapted from Sahai et al. (2015) [17]).

3. Accretion Activity or Chromospheric Emission

3.1. Models of Chromospheric Emission

We now investigate the question of what mechanism best explains the high-energy emission–accretion activity in a binary or chromospheric emission. The studies above strongly indicate that when $R_{fuv/nuv}$ is high, the origin of the high-energy emission is accretion activity. However, when it is low, either or both of these mechanisms may be responsible. Sahai et al. 2015 [17] show that if the X-ray luminosity $L_x > 0.001 L_\odot$, as found for their sample of fuvAGB stars, it is too high to arise in an MS companion’s corona. Similarly, the observed FUV emission in AGB stars ($\gtrsim 10 \mu\text{Jy}$, see below) is too high to arise in an MS companion’s chromosphere. The FUV flux of an MS Sun-like companion with a luminosity of, e.g., $\sim 1 L_\odot$, at the typical distances of AGB stars, > 100 pc, is $< 0.1\text{--}0.01 \mu\text{Jy}$, taking $(FUV/F_{bol}) \sim 10^{-4}\text{--}10^{-5}$ (see Figure 5 panels c,d of Viswanath et al. 2020 [23]; FUV is the UV flux integrated over the GALEX FUV bandpass, and F_{bol} is the bolometric flux).

We address this question by first considering the UV properties of a large sample of ~ 3500 AGB stars with spectral types M4 or later. This sample was constructed using the Hipparcos database as follows. First, we selected all stars with spectral type M (field H69 of the main Hipparcos catalog). From this list, we chose only those which simultaneously satisfied the color conditions: $V - I > B - V$, $B - V > 1$, and $V - I > 1.5$, allowing us to remove misclassified stars which were of intrinsically earlier spectral types. Finally, main-sequence M stars were removed by rejecting stars with parallaxes $\pi > 20$ mas: since the limiting V magnitude of Hipparcos is ~ 12.4 , any main-sequence M star (with a typical absolute magnitude of $M_V \sim 9$) would not be detectable at distances $\gtrsim 50$ pc. We found that

>20% were detected in one or both of the GALEX FUV and NUV bands, and about >9% were detected in both. These percentages are lower limits because most of the GALEX data come from the All-Sky Imaging Survey (AIS), which had relatively short exposure times, $\sim(1 - few) \times 100$ s.

The mean FUV (f_{FUV}) and NUV (f_{NUV}) for all stars in the database which were detected in both these bands (316 objects) show a linear relationship—we find that $f_{FUV} = R_{FUV/NUV} \times f_{NUV}$ provides a good fit to the bulk of the data, with $R_{FUV/NUV} = 0.061 \pm 0.0015$. Outliers, defined as data where the observed f_{FUV} value was $\geq 5\sigma$ away from the model fit, were removed iteratively until the slope and number of outliers converged (in six iterations), resulting in the removal of 17 outliers. Restricting our dataset to objects where the SNR for both the mean FUV and NUV was ≥ 5 (a total of 184 objects: Figure 5) did not affect the results significantly—we found $R_{FUV/NUV} = 0.060 \pm 0.0022$ after five iterations, with 14 outliers. We show below that models of chromospheric emission can explain $R_{fuv/nuv} \lesssim 0.06$: thus the outliers for which $R_{fuv/nuv}$ is significantly above 0.06 are objects where accretion activity is likely responsible for the UV emission, and the outliers for which $R_{fuv/nuv}$ is significantly below 0.06 are objects where chromospheres are weak or absent.

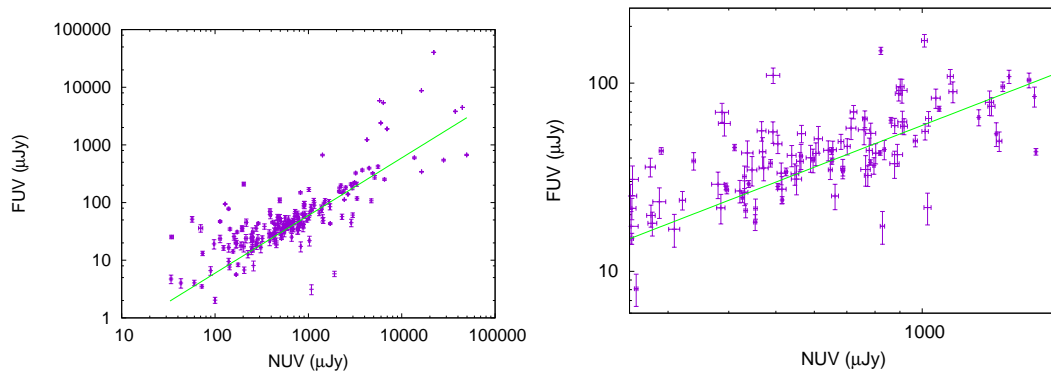


Figure 5. (Left) The mean FUV- and NUV-band fluxes of AGB stars observed with GALEX, for sources that were detected in both UV bands with a signal-to-noise ratio, $SNR \geq 5$. The green line shows a linear least-squares fit with outlier rejection, $f_{FUV} = R_{FUV/NUV} * f_{NUV}$, with $R_{FUV/NUV} = 0.06 \pm 0.002$. (Right) An expanded view of the central region is shown in the plot on the (Left).

We made a large grid of simple chromospheric models ($\sim 50,000$) using the CLOUDY code (Ferland et al. 2017 [24]) to compute the UV emission from a collisionally ionized plasma with temperature T_{chrom} and density nH contained within a layer of gas of thickness ΔR surrounding the AGB star. We show the observed $R_{fuv/nuv}$ versus the FUV-to-K band flux ratio for our sample of UV-emitting AGB stars, $R_{FUV/K}$, together with model values, in Figure 6—the latter is a good proxy for the fractional FUV luminosity, since the K-band flux is expected to result almost entirely from the emission from the AGB photosphere, excluding the effect of the presence of dust that may be present in a stellar wind.

We found that our chromosphere models can produce $R_{fuv/nuv} \sim 0.06$ for temperatures in the range $9000 \leq T_{chrom} (K) \leq 11,000$. Higher values of $R_{fuv/nuv}$ require higher temperatures, e.g., for $R_{fuv/nuv} \sim 0.1$, it requires $11,000 \leq T_{chrom} (K) \leq 15,000$. The allowed values of the parameters nH and ΔR are not independent, because the total emission from a collisionally excited plasma (as assumed for the CLOUDY models) is expected to be proportional to the square of the density and the total volume of emitting material. We found that for $0.2 \times 10^{-6} \lesssim (FUV/K) \lesssim 0.3 \times 10^{-6}$, where most of the AGB stars are located (Figure 6), the typical values of nH and ΔR were $10^{8.5} \text{ cm}^{-3}$ and 0.5 au, respectively, for a typical AGB star of radius 1.5 au.

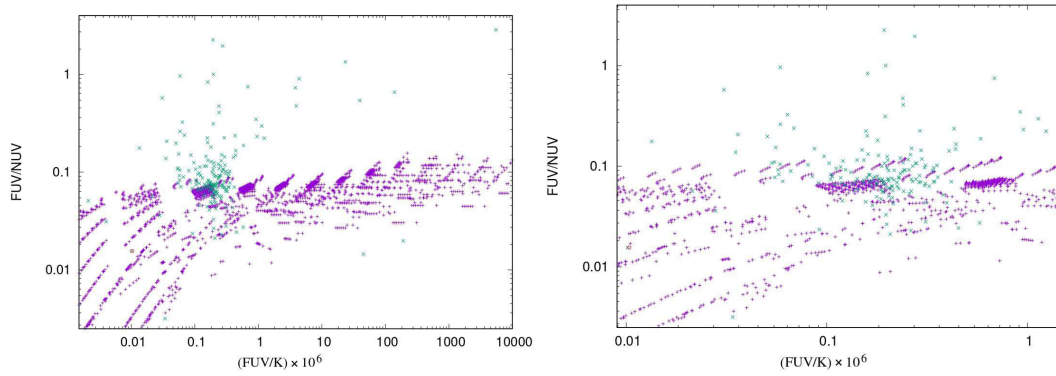


Figure 6. (Left) The observed (green symbols) and model (purple symbols) FUV/NUV flux ratio, $R_{FUV/NUV}$, versus the FUV/K-band (2MASS) flux ratio, for AGB stars that were detected in both UV bands with SNR of ≥ 5 . (Right) An expanded view of the central region in the plot on the (Left).

We compared our model results to the detailed chromospheric models for the M6 AGB star, g Her by Luttermoser et al. (1994) [25], based on fitting near-UV lines from the IUE data, with the greatest weight given to the Mg II *h* and *k* doublet (~ 2800 Å), followed by Mg I ($\lambda 2852$ Å) and the CII] UV0.01 multiplet (~ 2325 Å). The temperature distribution of their best-fit model, T10, ranged from 11,270 K to 3200 K. The model chromospheric layer extended from the photosphere to a height of ~ 1.7 au, with temperatures in the range ~ 9000 – $11,270$ K at heights $\gtrsim 0.45$ au. Our simple models thus appear to be a reasonable approximation to a more detailed model of the chromosphere for the purpose of investigating the dependence of $R_{fuv/nuv}$ on T_{chrom} .

3.2. Search for X-ray Emission from nuvAGB Stars

We also carried out a small survey of bright nuvAGB stars with XMM-Newton, i.e., stars with $R_{fuv/nuv} < 0.08$. Out of the seven targets proposed, two were observed, TW Hor and ϵ Oct. We found the somewhat surprising result that TW Hor, which has $R_{fuv/nuv} = 0.044$, was detected, whereas ϵ Oct, which has a higher value of $R_{fuv/nuv}$ (0.057), was not. An APEC model fit to the X-ray spectra of TW Hor showed that $T_x \sim 10^7$ K and $L_x \sim 0.0003 L_\odot$, most likely thermal emission from coronal gas (Figure 7a).

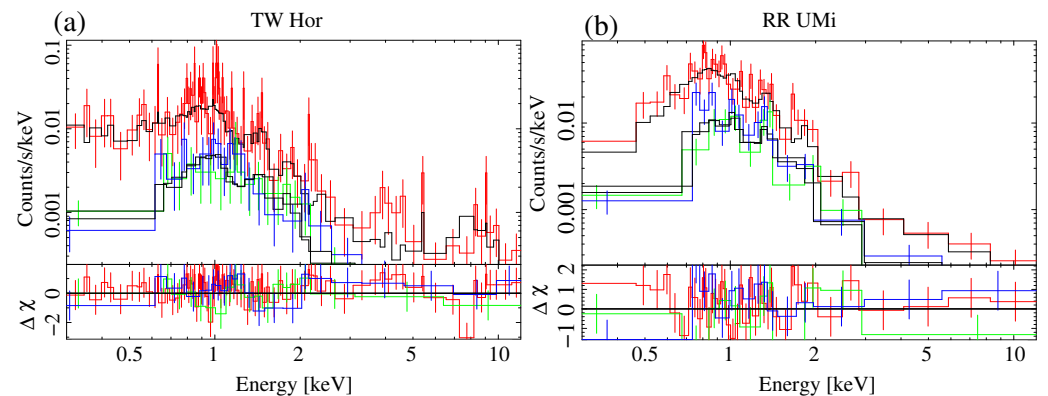


Figure 7. (a) X-ray spectra (EPIC/XMM) (colored curves) and APEC model fits (black curves) for (a) the nuvAGB star TW Hor, and (b) the fuvAGB star RR UMi. Bottom panel shows residuals.

Since AGB stars are unlikely to have sufficiently strong magnetic fields to confine the hot plasma, it is likely that the coronal gas in nuvAGB stars is associated with a main-sequence companion. These results suggest that a significant fraction of AGB stars with low FUV/NUV ratios, such as those with high FUV/NUV ratios, are also binaries. The soft X-ray component in such stars may be coronal emission from a main-sequence companion; if this hypothesis is correct, then we should expect to find examples of objects which show

X-ray emission from both the companion's corona as well as accretion activity. RR UMi (sp. type M5), with $R_{fuv/nuv} = 0.29$, is a plausible example. It shows X-ray emission that is best-fitted with a two-component APEC model, with the dominant component being soft, with $T_x \sim 6.6 \times 10^6$ K, resulting from the companion's corona and a secondary, harder component, with $T_x \sim 10^8$ K, due to accretion activity (Figure 7b).

4. Summary and Conclusions

Binarity interactions and accretion are now widely believed to play a major role in the death throes of most stars in the Universe that evolve in a Hubble time. UV and X-ray studies of AGB stars have now begun to provide robust observational evidence for binarity and associated accretion activity. Our main results are:

- A survey of ~ 3500 galactic AGB stars (sp. types M4–M10) reveals that a significant fraction of this population show UV emission ($\gtrsim 9\%$ NUV and FUV, and $\gtrsim 20\%$ NUV).
- The UV emission is variable, indicative of variable accretion activity, presumably due to a binary companion; this inference is supported by a detailed spectroscopic study of the star Y Gem.
- For stars with $R_{fuv/nuv} \gtrsim 0.06$, simple chromosphere models cannot produce the observed UV emission, and accretion activity in a binary is the most likely mechanism for UV emission (supported by X-ray studies).
- For stars with $R_{fuv/nuv} \lesssim 0.06$, simple chromosphere models can produce the observed UV emission; however the, X-ray detection of one out of two such stars suggests that some fraction of these may also be in binary systems but with low accretion rates.

Author Contributions: Conceptualization, R.S.; methodology, R.S., J.S.-F., M.G., R.O. and C.S.C.; software, R.S.; formal analysis, R.S., J.S.-F. and M.G.; writing—original draft preparation, review and editing, R.S.; funding acquisition, R.S. All authors have read and agreed to the published version of the manuscript.

Funding: R.S.'s contribution to this research was funded in part by NASA via ADAP awards, and multiple HST GO awards from the Space Telescope Science Institute. C.S.C.'s contribution was supported through I+D+i project ID PID2019-105203GB-C22 funded by the Spanish MCIN/AEI/10.13039/501100011033. J.S.-F.'s contribution was supported through project ID PID2019-109522GB-C51 funded by the Spanish MCIN/AEI/10.13039/501100011033.

Data Availability Statement: All the data reported in this study, except the X-ray data on TW Hor and ϵ Oct, are available from the XMM-Newton, Chandra X-ray Observatory, and GALEX archives.

Acknowledgments: R.S.'s contribution to the research described here was carried out at the Jet Propulsion Laboratory, California Institute of Technology, under a contract with NASA.

Conflicts of Interest: The authors declare no conflict of interest. The funders had no role in the design of the study; in the collection, analyses, or interpretation of data; in the writing of the manuscript, or in the decision to publish the results.

References

1. Decin, L. Evolution and Mass Loss of Cool Ageing Stars: A Daedalean Story. *Annu. Rev. Astron. Astrophys.* **2021**, *59*, 337–389. [[CrossRef](#)]
2. Olofsson, H. The study of evolved stars with ALMA. *Astrophys. Space Sci.* **2008**, *313*, 201–207. [[CrossRef](#)]
3. Sahai, R.; Trauger, J.T. Multipolar Bubbles and Jets in Low-Excitation Planetary Nebulae: Toward a New Understanding of the Formation and Shaping of Planetary Nebulae. *Astron. J.* **1998**, *116*, 1357–1366. [[CrossRef](#)]
4. Sahai, R.; Morris, M.; Sánchez Contreras, C.; Claussen, M. Preplanetary Nebulae: A Hubble Space Telescope Imaging Survey and a New Morphological Classification System. *Astron. J.* **2007**, *134*, 2200–2225. [[CrossRef](#)]
5. Sahai, R.; Morris, M.R.; Villar, G.G. Young Planetary Nebulae: Hubble Space Telescope Imaging and a New Morphological Classification System. *Astron. J.* **2011**, *141*, 134–164. [[CrossRef](#)]
6. Bujarrabal, V.; Castro-Carrizo, A.; Alcolea, J.; Sánchez Contreras, C. Mass, linear momentum and kinetic energy of bipolar flows in protoplanetary nebulae. *Astron. Astrophys.* **2001**, *377*, 868–897. [[CrossRef](#)]
7. Sahai, R.; Morris, M.; Sánchez Contreras, C.; Claussen, M. Normal, Nascent and Stalled Pre-Planetary Nebulae. *Planet. Nebul. Our Galaxy Beyond* **2006**, *234*, 499–500. [[CrossRef](#)]

8. Ivanova, N.; Justham, S.; Chen, X.; De Marco, O.; Fryer, C.L.; Gaburov, E.; Ge, H.; Glebbeek, E.; Han, Z.; Li, X.-D.; et al. Common envelope evolution: Where we stand and how we can move forward. *Astron. Astrophys. Rev.* **2013**, *21*, 59–141. [[CrossRef](#)]
9. Soker, N. Close Stellar Binary Systems by Grazing Envelope Evolution. *Astrophys. J.* **2015**, *800*, 114. [[CrossRef](#)]
10. Blackman, E.G.; Frank, A.; Markiel, J.A.; Thomas, J.H.; Van Horn, H.M. Dynamos in asymptotic-giant-branch stars as the origin of magnetic fields shaping planetary nebulae. *Nature* **2001**, *409*, 485–487. [[CrossRef](#)]
11. Blackman, E.G.; Lucchini, S. Using kinematic properties of pre-planetary nebulae to constrain engine paradigms. *Mon. Not. R. Astron. Soc.* **2014**, *440*, L16–L20. [[CrossRef](#)]
12. Wood, P.R.; Alcock, C.; Allsman, R.A.; Alves, D.; Axelrod, T.S.; Becker, A.C.; Bennett, D.P.; Cook, K.H.; Drake, A.J.; Freeman, K.C.; et al. MACHO observations of LMC red giants: Mira and semi-regular pulsators, and contact and semi-detached binaries. In *Symposium-International Astronomical Union*; Cambridge University Press: Cambridge, UK, 1999; Volume 191, pp. 151–158.
13. Soszyński, I.; Olechowska, A.; Ratajczak, M.; Iwanek, P.; Skowron, D.M.; Mróz, P.; Pietrukowicz, P.; Udalski, A.; Szymański, M.K.; Skowron, J.; et al. Binarity as the Origin of Long Secondary Periods in Red Giant Stars. *Astrophys. J.* **2021**, *911*, L22. [[CrossRef](#)]
14. Sahai, R.; Findeisen, K.; de Paz, A.G.; Sánchez Contreras, C. Binarity in Cool Asymptotic Giant Branch Stars: A GALEX Search for Ultraviolet Excesses. *Astrophys. J.* **2008**, *689*, 1274–1278. [[CrossRef](#)]
15. Ortiz, R.; Guerrero, M.A. Ultraviolet emission from main-sequence companions of AGB stars. *Mon. Not. R. Astron. Soc.* **2016**, *461*, 3036–3046. [[CrossRef](#)]
16. Sahai, R.; Sánchez Contreras, C.; Mangan, A.S.; Sanz-Forcada, J.; Muthumariappan, C.; Claussen, M.J. Binarity and Accretion in AGB Stars: HST/STIS Observations of UV Flickering in Y Gem. *Astrophys. J.* **2018**, *860*, 105. [[CrossRef](#)]
17. Sahai, R.; Sanz-Forcada, J.; Sánchez Contreras, C.; Stute, M. A Pilot Deep Survey for X-ray Emission from fuvAGB Stars. *Astrophys. J.* **2015**, *810*, 77. [[CrossRef](#)]
18. Kastner, J.H.; Soker, N. Constraining the X-ray Luminosities of Asymptotic Giant Branch Stars: TX Camelopardalis and T Cassiopeia. *Astrophys. J.* **2004**, *608*, 978–982. [[CrossRef](#)]
19. Ortiz, R.; Guerrero, M.A. X-ray AGB Stars in the 4XMM-DR9 Catalog: Further Evidence for Companions. *Astrophys. J.* **2021**, *912*, 93. [[CrossRef](#)]
20. Smith, R.K.; Brickhouse, N.S.; Liedahl, D.A.; Raymond, J.C. Collisional plasma models with APEC/APED: Emission-line diagnostics of hydrogen-like and helium-like ions. *Astrophys. J.* **2001**, *556*, L91. [[CrossRef](#)]
21. Ramstedt, S.; Montez, R.; Kastner, J.; Vlemmings, W.H.T. Searching for X-ray emission from AGB stars. *Astron. Astrophys.* **2012**, *543*, A147. [[CrossRef](#)]
22. Montez, R.; Ramstedt, S.; Kastner, J.H.; Vlemmings, W.; Sanchez, E. A Catalog of GALEX Ultraviolet Emission from Asymptotic Giant Branch Stars. *Astrophys. J.* **2017**, *841*, 33. [[CrossRef](#)]
23. Viswanath, G.; Narang, M.; Manoj, P.; Mathew, B.; Kartha, S.S. A Statistical Search for Star-Planet Interaction in the Ultraviolet Using GALEX. *Astron. J.* **2020**, *159*, 194. [[CrossRef](#)]
24. Ferl, G.J.; Chatzikos, M.; Guzmán, F.; Lykins, M.L.; Van Hoof, P.A.M.; Williams, R.J.R.; Abel, N.P.; Badnell, N.R.; Keenan, F.P.; Porter, R.L.; et al. The 2017 Release Cloudy. *Rev. Mex. Astron. Astrofis.* **2017**, *53*, 385–438.
25. Luttermoser, D.G.; Johnson, H.R.; Eaton, J. The Chromospheric Structure of the Cool Giant Star G Herculis. *Astrophys. J.* **1994**, *422*, 351. [[CrossRef](#)]